Novel and Reusable Magnetic Zinc Ferrites Modified SBA-15 Supported Ionic Liquids for Sustainable and Efficient Cycloaddition of CO$_2$ and Epoxides to Cyclic Carbonates

Yu Lin Hu[1]*, Zhi Guo Sun[1], Xiao Bing Liu[2]

[1]College of Chemistry and Chemical Engineering, Anshun University, Anshun 561000, P. R. China.
[2]College of Chemistry and Chemical Engineering, Jinggangshan University, Ji'an 343009, P. R. China.

*Corresponding author: Yu Lin Hu, email: huyulin1982@163.com

Abstract. A type of magnetic zinc ferrites modified SBA-15 supported ionic liquids have been synthesized and evaluated as effective catalysts for the synthesis of cyclic carbonates from epoxides and CO$_2$. The effects of catalysts, CO$_2$ pressure, reaction temperature, and catalyst stability have also been investigated, the catalyst ZnFe$_2$O$_4$@SBA-15-ILVO$_3$ exhibited excellent activity in high to excellent yields (87~98 %) with excellent selectivities (98~99.7 %). Moreover, the catalyst exhibited excellent stability and could be easily recovered and reused for five times without a considerable decrease in catalytic activity. This work provides a sustainable and efficient strategy for the chemical fixation of carbon dioxide into valuable cyclic carbonates.
Keywords: Supported ionic liquid; magnetic zinc ferrites modified SBA-15; cycloaddition; cyclic carbonates; carbon dioxide.

Resumen. Se sintetizó y evaluó un líquido iónico soportado tipo ferrita de zinc magnética modificada SBA-15 como un catalizador efectivo para la síntesis de carbonatos cíclicos a partir de epóxidos y CO$_2$. Se investigaron los efectos del catalizador, el CO$_2$, la presión, la temperatura de reacción y la estabilidad del catalizador; el catalizador ZnFe$_2$O$_4$@SBA-15-ILVO$_3$ mostró una excelente actividad con rendimientos de altos a excelentes (87~98 %), así como excelentes selectividades. Adicionalmente, el catalizador mostró tener una excelente estabilidad, y se logró recuperar y reutilizar fácilmente en cinco ocasiones sin mostrar un decremento importante en su actividad catalítica. Este trabajo proporciona una estrategia sostenible y eficiente para la transformación química de dióxido de carbono en carbonatos cíclicos de alto valor.
**Palabras clave:** Líquidos iónicos soportados; ferritas de zinc magnéticas modificadas SBA-15; cicloadición; carbonatos cíclicos; dióxido de carbono.

Introduction

Chemical fixation of CO$_2$ into value-added products was one of the promising strategies for CO$_2$ capture and storage, which play important roles towards the clean environment [1-4]. As a promising way for CO$_2$ chemical utilization, the cycloaddition reaction of CO$_2$ with epoxides is promising due to both the view of 100% atomic economy and the wide applications of cyclic carbonates products in fine chemistry and industry [5,6]. However, due to the thermodynamic stability and kinetic inertness of CO$_2$, considerable efforts have been devoted to develop efficient catalytic systems for the CO$_2$ sustainable transformation. Recently, a wide range

of catalytic systems have been successfully developed for the synthesis of cyclic carbonates, including metal complexes [7-9], metal-organic frameworks [10-12], covalent organic frameworks [13,14], $InBr_3$/NBu_4Br [15], Ag/TUD-1 [16], organocatalysts [17-19], Zn–Zr bimetallic oxide [20], and others [21-23]. Despite these advances, the development of a green and sustainable strategy for the chemical fixation of CO_2 into cyclic carbonates via the cycloaddition with epoxides remains a challenge for chemists.

Ionic liquids (ILs) have found numerous applications in various areas of reaction solvents and catalysis due to their negligible vapour pressure, thermal and chemical stability, non-flammable, nonvolatile, low toxicity and strong structural design prospects [24-28]. Through the functional design of anions and cations of ionic liquids, the use of ILs as catalysts in the efficient synthesis of cyclic carbonates via the cycloaddition of CO_2 and epoxides have been developed [29-31]. However, the isolation of pure ILs from products and reusability has been the major issue in these processes in view of eco-sustainability. Immobilization of ILs onto solid supports could alleviate these issues, not only reduce cost, and enhance catalytic efficiency, but also facilitate catalyst separation and reutilization [32-35]. Amongst the available supports, magnetic mesoporous materials such as the inactive mesoporous silica materials modified by different magnetic active metal oxides have become as exceptional and significant solid supports due to the unique properties of high specific surface area, easy functionalization, well-defined size, controlled pore size distribution, innocuity and high biocompatiblity, good hydrothermal stability as well as easy separation and reusability [36-46]. Herein, a type of magnetic zinc ferrites modified SBA-15 supported ionic liquids via the immobilization of different amounts of functional ionic liquids onto active magnetic zinc ferrites modified SBA-15 supports have been designed to investigate their catalytic performance in the synthesis of cyclic carbonates via the cycloaddition of CO_2 and epoxides under mild conditions (Scheme 1). In addition, catalyst reusability was also carried out to assess the stability of the catalytic system.
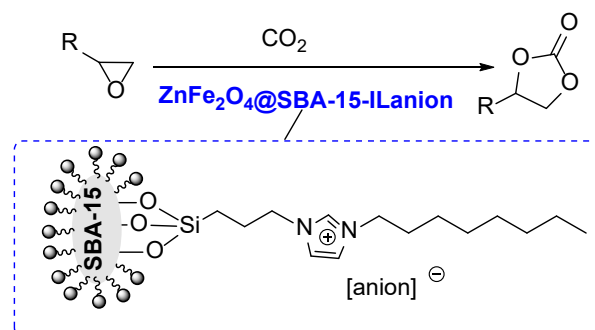
Scheme 1. Catalytic synthesis of cyclic carbonates with magnetic supported ionic liquids.

Experimental

Materials and apparatus

Pluronic 123 ($EO_{20}PO_{70}EO_{20}$) was purchased from Sigma-Aldrich, and other reagents are of analytical grade and used directly without further purification. Scanning electron microscopy (SEM) and energy dispersive X-ray spectroscopy (EDX) were recorded with a JSM-7500F electron microscope. FT-IR spectra were conducted on a PE Fourier Transform spectrometer in a range from 4000 to 400 cm^{-1}. Powder X-ray diffraction patterns were recorded on an Ultima IV diffractometer using Cu Kα radiation (λ = 1.5405 Å), with a scan speed of 4°/min. Thermogravimetric analysis (TGA) was performed on a NETZSCH STA 449 F5 with a heating rate of 10 °C min^{-1} under nitrogen. UV-Vis spectra were obtained on a Shimadzu UV-2450 spectrophotometer. The BET surface area and pore volume distributions of the catalysts were determined with N_2 adsorption-desorption isotherms using a BELSORP-max instrument. Pore size distribution curves were calculated from the analysis of desorption branch of the isotherm by the BJH (Barrett–Joyner–Halenda). Magnetic properties were carried out using a vibrating sample magnetometer (PPMS-9T, Quantum Design, USA) in the magnetic field range of -10000 to 10000 Oe at room temperature. ^1H NMR spectra were recorded

on a Bruker Avance 400 MHz spectrometer in DMSO-d_6 or $CDCl_3$ with tetramethylsilane (TMS) as an internal reference. Elemental analysis were obtained on a Vario Micro cube Elemental Analyzer. Melting points were measured by an electro-thermal IA 9100 apparatus.

Synthesis of magnetic supported ionic liquids

Magnetic zinc ferrites functionalized SBA-15 support $ZnFe_2O_4$@SBA-15 was synthesized following the previously reported methods [42-44]. The supported ionic liquids were prepared according to the similar procedures described in literatures (Scheme 2) [25-29, 36-39]. To a round-bottomed flask were added sodium ethoxide (0.3 mol), imidazole (0.3 mol) and ethanol (150 mL). The mixture was vigorously stirred at 70 °C for 8 h, then (3-chloropropyl) triethoxysilane (0.3 mol) was added into the solution gradually and stirred at 80 °C for 12 h. After filtering the slurry and evaporating the ethanol solvent to give **1**. Next, 1-bromo-octan (0.2 mol) and **1** (0.2 mol) were dispersed in 120 mL of toluene, and the resulting mixture was stirred under nitrogen at 110 °C for 24 h. After this procedure, the excess solvent was isolated by liquid-liquid separation and the residue was dried under vacuum at 70 °C to give **2**. Then, **2** (0.1 mol), potassium metavanadate (0.1 mol) or sodium dihydrogen citrate (0.1 mol) or sodium proline (0.1 mol), and methanol (60 mL) were refluxed under vigorous stirring for 24 h. The suspension was filtered, washed with ethanol and dried at 50 °C to give the anionic functionalized ionic liquids ILanion **3**. Finally, the magnetic supported ionic liquids **4** were synthesized using a post-synthesis grafting method. A mixture of the as-prepared $ZnFe_2O_4$@SBA-15 (2.0 g), ILanion **3** (1.2 g), and ethanol (80 mL) was refluxed for 24 h. The resulting precipitates were centrifugalized, washed three times with dichloromethane and dried at 50 °C overnight to obtain $ZnFe_2O_4$@SBA-15-ILanion **4**.
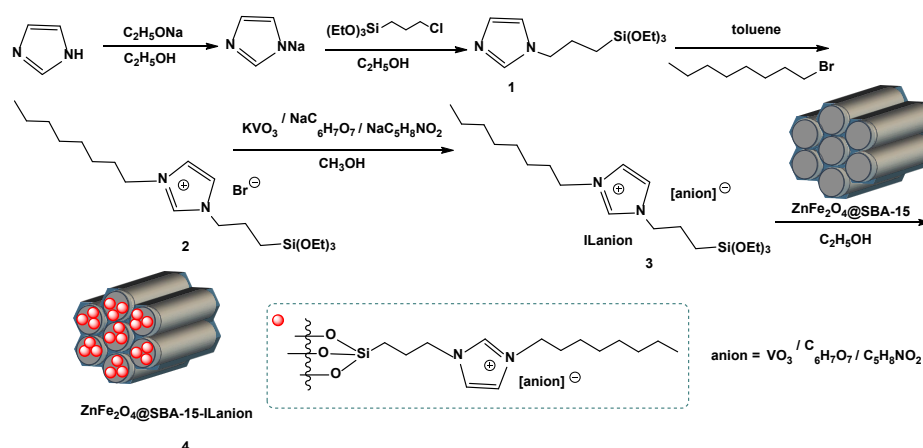
Scheme 2. Synthesis of magnetic supported ionic liquids.

Catalytic synthesis of cyclic carbonates

The cycloaddition reactions of CO_2 and epoxides were conducted in a stainless-steel autoclave. Typically, the reaction autoclave was replaced with CO_2, then epoxide (10 mmol) and $ZnFe_2O_4$@SBA-15-$ILVO_3$ (0.15 g) were added into the autoclave under stirring. The reaction mixture was stirred at 90 °C for a desired time under a fixed pressure. The reaction progress was monitored by GC. After completion of the reaction, the catalyst was easily separated by an external magnet and then washed three times with CH_2Cl_2 for the recycling experiments, fresh substrates were added and recycled under identical reaction conditions. All target products are known and commercial, thus were verified by comparison with those of standard compounds or by ^1H NMR and Elemental analysis.

Spectroscopic data for products

1,3-Dioxolan-2-one (Table 2, entry 1). ^1H NMR (400 MHz, $CDCl_3$) (δ/ppm): 4.53 (s, CH_2, 2H). Elemental analysis for $C_3H_4O_3$: C, 40.84; H, 4.53; O, 54.44. Found: C, 40.92; H, 4.58; O, 54.50.

Propylene carbonate (Table 2, entry 2). ^{1}H NMR (400 MHz, CDCl$_3$) (δ/ppm): 1.47 (dd, CH$_3$, 3H), 3.95 (t, CH, 1H), 4.53 (t, CH, 1H), 4.82 (m, CH, 1H); Elemental analysis for C$_4$H$_6$O$_3$: C, 47.01; H, 5.86; O, 46.97. Found C, 47.06; H, 5.92; O, 47.01.

(Chloromethyl)ethylene carbonate (Table 2, entry 3). ^{1}H NMR (400 MHz, CDCl$_3$) (δ/ppm): 3.75 (dd, CH$_2$, 2H), 4.32 (t, CH$_2$, 1H), 4.59 (t, CH$_2$, 1H), 4.93 (m, CH, 1H); Elemental analysis for C$_4$H$_5$ClO$_3$: C, 35.14; Cl, 25.92; O, 35.11. Found C, 35.19; Cl, 25.96; O, 35.15.

4-(Hydroxymethyl)-1,3-dioxolan-2-one (Table 2, entry 4). ^{1}H NMR (400 MHz, CDCl$_3$) (δ/ppm): 3.56 (t, CH$_2$, 2H), 4.28-4.50 (dd, CH$_2$, 2H), 4.76 (m, CH, 1H), 5.25 (t, OH, 1H). Elemental analysis for C$_4$H$_6$O$_4$: C, 40.64; H, 5.07; O, 54.15. Found: C, 40.68; H, 5.12; O, 54.19.

1,2-Butylene glycol carbonate (Table 2, entry 5). ^{1}H NMR (400 MHz, CDCl$_3$) (δ/ppm): 0.93 (t, CH$_3$, 3H), 1.57-1.61 (m, CH$_2$, 2H), 4.06 (t, CH$_2$, 2H); 4.42 (d, CH$_2$, 1H); 4.64 (m, CH, 1H); Elemental analysis for C$_5$H$_8$O$_3$: C, 51.68; H, 6.90; O, 41.32. Found: C, 51.72; H, 6.94; O, 41.34.

Hexahydrobenzo[d][1,3]dioxol-2-one (Table 2, entry 6). ^{1}H NMR (400 MHz, CDCl$_3$) (δ/ppm): 1.37-1.42 (m, CH$_2$CH$_2$, 4H), 1.74-1.80 (m, 2CH$_2$, 4H), 4.61 (t, 2CH, 2H); Elemental analysis for C$_7$H$_{10}$O$_3$: C, 59.11; H, 7.05; O, 33.71. Found C, 59.15; H, 7.09; O, 33.76.

Styrene carbonate (Table 2, entry 7). ^{1}H NMR (400 MHz, CDCl$_3$) (δ/ppm): 4.30 (t, CH$_2$, 1H), 4.72 (t, CH$_2$, 1H), 5.67 (t, CH$_2$, 1H), 7.29-7.37 (m, Ar-H, 5H); Elemental analysis for C$_9$H$_8$O$_3$: C, 65.80; H, 4.86; O, 29.21. Found C, 65.85; H, 4.91; O, 29.24.

Results and discussion

X-ray diffraction (XRD) was performed to investigate the structure of the supported ionic liquids. As can be seen from the Fig. 1, all the samples exhibited a broad diffraction peak between 2θ = 20-25°, which are assigned to the characteristic peak of mesoporous silica [42-45], suggesting the basic crystalline structure of ordered mesoporous materials. The characterization peaks at 2θ = 30.3°, 35.4°, 42.8°, 53.6, 56.5°, 62.4° assigned to the ZnFe$_2$O$_4$ crystal planes (220), (311), (400), (422), (511), (440), respectively (JCPDS card No. 221012). In addition, no obvious peaks about the ionic liquid species were observed, indicating a well dispersion on the support framework.
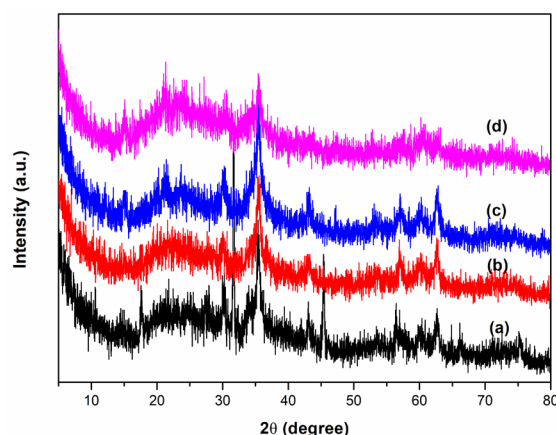

Fig. 1. XRD diffractograms of ZnFe2O4@SBA-15-ILVO3 **(a)**, ZnFe2O4@SBA-15-ILC6H7O7 **(b)**, ZnFe2O4@SBA-15-ILC5H8NO2 **(c)**, and ZnFe2O4@SBA-15 **(d)**.

The surface morphologies of samples are evaluated by SEM analysis. As shown in Fig. 2**(d)**, ZnFe$_2$O$_4$@SBA-15 presents an irregular shape consisting of some spherical agglomerates with wrinkled nano-sized particles. Fig. 2**(a-c)** display the SEM images of the magnetic supported ionic liquids. After the immobilization of ionic liquid on the ZnFe$_2$O$_4$@SBA-15 support, the whole morphologies are retained, pointing to the preservation of the well-ordered structure in these supported ionic liquids. Comparatively, the typical aggregated small and irregular particles are clearly seen in these samples, which are attributed to the IL immobilization results. The EDX analysis revealed the presence of the corresponding elemental signals including C, Si, O, N, V, Fe, Zn in these supported ionic liquids (Fig. 3), indicating the successful immobilization of ionic liquid moieties on the support framework.
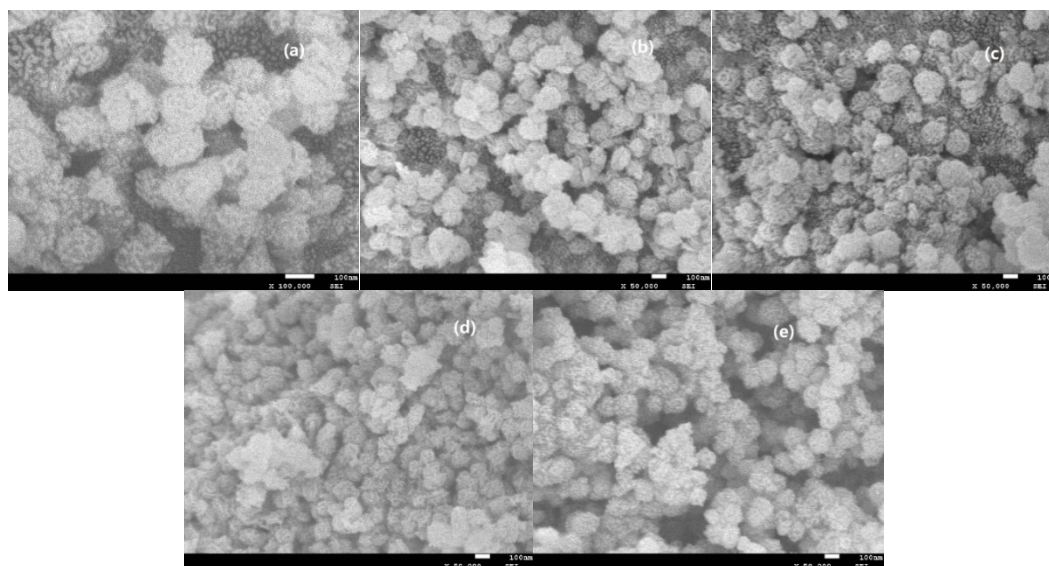
Fig. 2. SEM images of ZnFe2O4@SBA-15-ILVO3 **(a)**, ZnFe2O4@SBA-15-ILC6H7O7 **(b)**, ZnFe2O4@SBA-15-ILC5H8NO2 **(c)**, and ZnFe2O4@SBA-15 **(d)**, five times recycled ZnFe2O4@SBA-15-ILVO3 **(e)**.
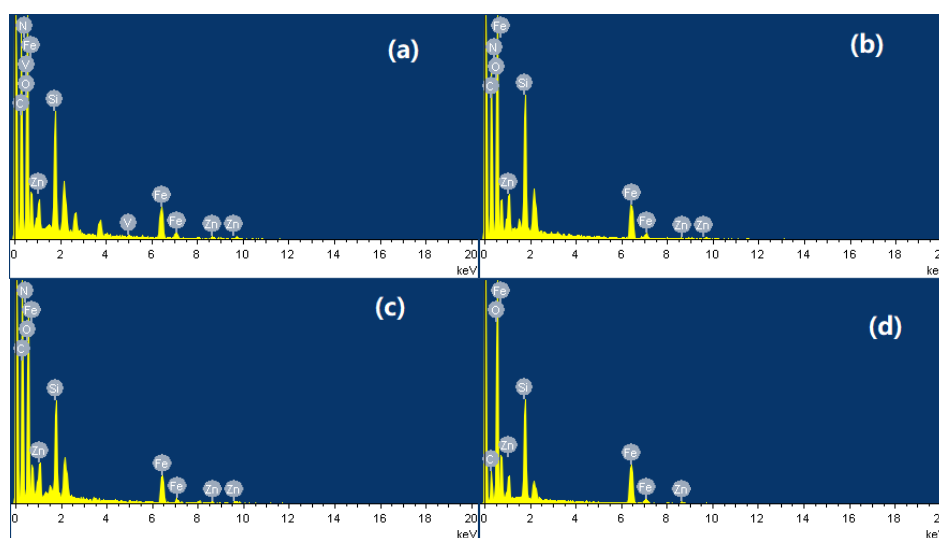
Fig. 3. EDX images of ZnFe2O4@SBA-15-ILVO3 **(a)**, ZnFe2O4@SBA-15-ILC6H7O7 **(b)**, ZnFe2O4@SBA-15-ILC5H8NO2 **(c)**, and ZnFe2O4@SBA-15 **(d)**.

To validate and characterize the functional groups of the supported ionic liquids, FT-IR spectra of the samples are taken. As shown in Fig. 4, the peak around 3600-3345 cm^{-1} was accounted for the characteristic band of hydroxyl stretching vibration. The peaks at around 2952-2853 cm^{-1} are attributed to the C-H stretching vibration of CH$_3$ and CH$_2$. The characteristic peaks at around 1085 cm^{-1} and 804 cm^{-1} are attributed to the Si-O-Si stretching vibration. The absorption peaks around 1634 cm^{-1}, and 1259 cm^{-1} are assigned to C=C, and C–N stretching vibrations of imidazole ring [25-27]. Also, the peak at around 725 cm^{-1} is attributed to bending vibration of CH$_2$ units. Furthermore, the peaks at about 575 cm^{-1}, and 417 cm^{-1} were assigned to the lattice vibration modes of ZnFe$_2$O$_4$ [41-43]. The above results indicated that the existence of mainly characteristic groups and the successful immobilization of ionic liquid on the support. The UV–vis spectra of the samples are shown in Fig. 5. For the supported catalysts, three major adsorption peaks could be observed in the region of 210-450 nm, the absorption peaks centered at around 227 nm is attributed to Si-O transition, other absorption weak peaks located at around 398 nm and 439 nm are probably assigned to the absorption of zinc ferrite particles of ZnFe$_2$O$_4$ [38-41]. At the same time, no remarkable peaks of ionic liquid are found on the UV–vis spectra of the supported ionic liquids, which might be due to their low loading and good dispersion on the support framework.
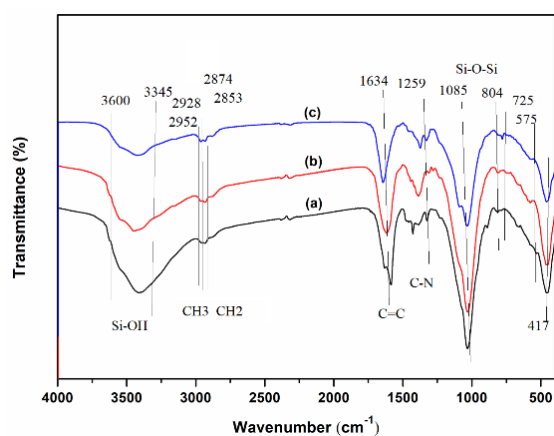

Fig. 4. FT-IR spectras of ZnFe2O4@SBA-15-ILVO3 **(a)**, ZnFe2O4@SBA-15-ILC6H7O7 **(b)**, ZnFe2O4@SBA-15-ILC5H8NO2 **(c)**.
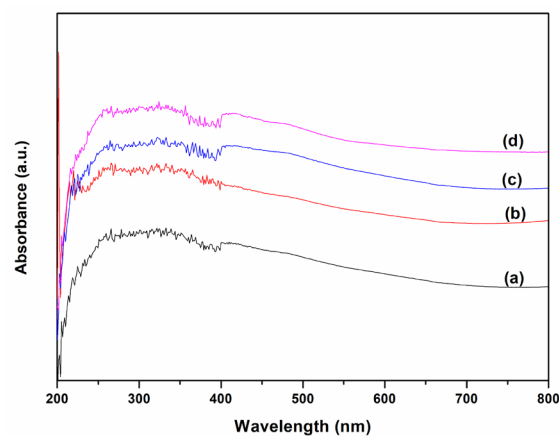
Fig. 5. UV–Vis spectras of ZnFe2O4@SBA-15-ILVO3 **(a)**, ZnFe2O4@SBA-15-ILC6H7O7 **(b)**, ZnFe2O4@SBA-15-ILC5H8NO2 **(c)**, and ZnFe2O4@SBA-15 **(d)**.

The structural characteristics of the superior supported catalysts $ZnFe_2O_4$@SBA-15-ILVO_3, and $ZnFe_2O_4$@SBA-15 are accomplished by a N_2 adsorption-desorption isotherms and BJH pore size distribution analysis. As shown in Fig. 6, these samples exhibit the type IV isotherms with H1 hysteresis loop at relative pressure $(P/P_0) = 0.5$-0.7, indicating their typical mesoporous structures. It is clearly found that the surface area and pore volume are significantly decreased from 145.7 m^2/g, 0.59 cm^3/g for $ZnFe_2O_4$@SBA-15, 80.2 m^2/g, 0.42 cm^3/g for $ZnFe_2O_4$@SBA-15-ILVO_3, respectively. The reduced surface area and pore volume may be due to the successful immobilization of ionic liquid on the support. Compared with the pure $ZnFe_2O_4$@SBA-15 support, the supported catalyst $ZnFe_2O_4$@SBA-15-ILVO_3 displayed no obvious change in terms of the pore size distribution (12.5 nm for $ZnFe_2O_4$@SBA-15, 12.8 nm for $ZnFe_2O_4$@SBA-15-ILVO_3). It is worth noting that after the loading of ionic liquid, the mesoporous structure of the catalyst can be well remained.

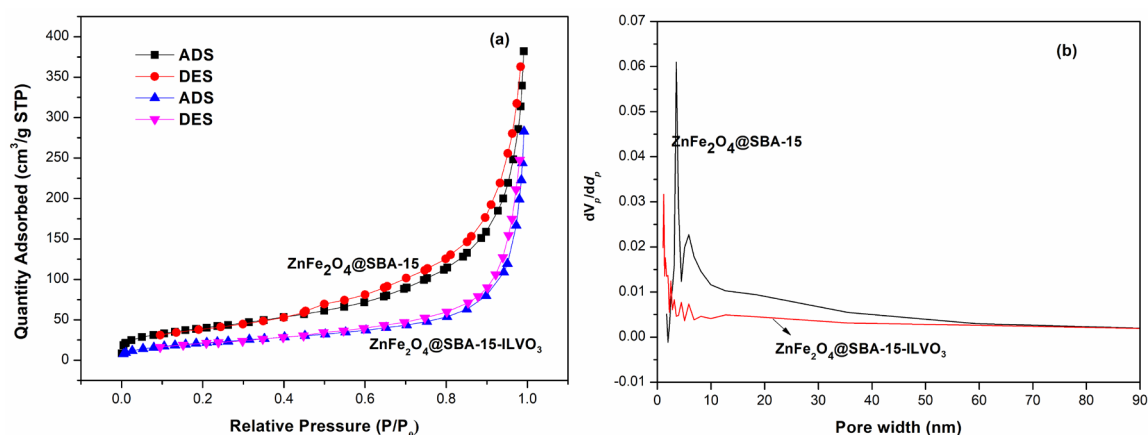**Fig. 6. (a)** N2 adsorption-desorption isotherms and **(b)** pore size distributions of ZnFe2O4@SBA-15, and ZnFe2O4@SBA-15-ILVO3.

Initially, the catalytic performance of the magnetic supported ionic liquids was investigated employing the cycloaddition of CO_2 and propylene oxide with as the model reaction, and the results were summarized in Table 1. In a first set of experiments, the reaction was carried out in the presence of the three supported ionic liquids catalysts of $ZnFe_2O_4$@SBA-15-ILC_6H_7O_7, $ZnFe_2O_4$@SBA-15-ILC_5H_8NO_2 and $ZnFe_2O_4$@SBA-15-ILVO_3 (Table 1, entries 1-3). It was observed that $ZnFe_2O_4$@SBA-15-ILVO_3 achieved the best outcome, in terms of 98 % yield of propylene carbonate with 99.5 % selectivity (Table 1, entry 3). For comparison, bare magnetic support $ZnFe_2O_4$@SBA-15 or bulk ionic liquids as catalysts in the cycloaddition gave much low product yields (48~75 %) and selectivities (90.5~93.7 %) (Table 1, entries 4-7). Besides these, no product was obtained when the reaction in the absence any catalyst (Table 1, entry 8). The influence of the amount of suitable catalyst $ZnFe_2O_4$@SBA-15-ILVO_3 on the cycloaddition was also studied. It can be seen that the product yield increased with increasing the amount of catalyst from 0.05 g to 0.15 g (Table 1, entries 9, 10 and 3). No significant enhancement in the yield was observed with further increasing the catalyst amount to 0.3 g (Table 1, entries 11 and 12). Thus, the optimum catalyst amount was 0.15 g.

Table 1. Catalyst screening for the cycloaddition of propylene oxide with CO_2.[a]

Entry	Catalyst	Catalyst (g)	Time (h)	Yield (%)[b]	Selectivity (%)[c]
1	$ZnFe_2O_4$@SBA-15-ILC_6H_7O_7	0.15	3	84	97.2
2	$ZnFe_2O_4$@SBA-15-ILC_5H_8NO_2	0.15	3	90	98.7
3	$ZnFe_2O_4$@SBA-15-ILVO_3	0.15	3	98	99.5

4	$ILC_6H_7O_7$	0.2	8	57	90.5
5	$ILC_5H_8NO_2$	0.2	8	69	92.1
6	$ILVO_3$	0.2	8	75	93.0
7	$ZnFe_2O_4@SBA-15$	0.4	8	48	93.7
8	-	-	24	trace	-
9	$ZnFe_2O_4@SBA-15-ILVO_3$	0.05	5	51	98.7
10	$ZnFe_2O_4@SBA-15-ILVO_3$	0.1	3	82	99.1
11	$ZnFe_2O_4@SBA-15-ILVO_3$	0.2	3	98	99.4
12	$ZnFe_2O_4@SBA-15-ILVO_3$	0.3	3	97	99.2

[a]Reaction conditions: propylene oxide (10 mmol), CO_2 (0.5 MPa), 90 °C. [b]Isolated yield. [c]GC analysis.

Then the influence of CO_2 pressure on the cycloaddition was also studied (Fig. 7**(a)**). It can be seen that the product yield and selectivity increased with increasing the CO_2 pressure from 0.2 MPa to 0.5 MPa. These results were related to the favorable diffusion between substrates and $ZnFe_2O_4@SBA-15-ILVO_3$ at the higher CO_2 pressures, resulting in more mass transfer and increasing the cycloaddition efficiency. No significant enhancement in the yield and selectivity was observed with further increasing the CO_2 pressure to 1.0 MPa. Excessive CO_2 pressure may reduce the concentration of propylene oxide, resulting in the slightly reduced product yield and selectivity. Thus, the optimum CO_2 pressure was 0.5 MPa. Moreover, reaction temperature was an important factor to affect the cycloaddition (Fig. 7**(b)**). It can be seen that the yield was increased in the reaction temperature up to 90 °C. Nevertheless, use of higher temperature beyond 90 °C would lead to a decreased yield and selectivity, which was due to the side reactions of isomerization and ring opening occurred at overly high temperatures (GC analysis). Accordingly, the appropriate temperature is 90 °C.
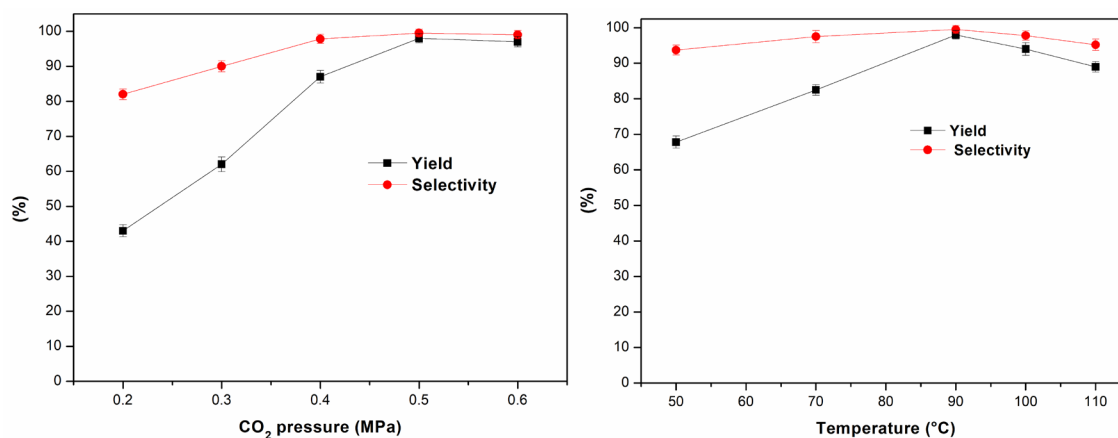

Fig. 7. (a) Influence of CO2 pressure on the cycloaddition (10 mmol propylene oxide, 0.15 g ZnFe2O4@SBA-15-ILVO3, 90 °C, 3 h), **(b)** influence of reaction temperature on the cycloaddition (10 mmol propylene oxide, 0.15 g ZnFe2O4@SBA-15-ILVO3, 0.5 MPa CO2, 3 h).

Furthermore, the thermal stability catalyst of $ZnFe_2O_4@SBA-15-ILVO_3$ was evaluated by thermogravimetric analysis (TGA) (Fig. 8**(a)**). The first weight loss of 5.4 % below 200 °C was attributed to the elimination of adsorbed water and solvent. The second weight loss of 20.06 % from 200 °C to 600 °C was

due to the elimination and decomposition of the ionic liquid moieties. This analysis strongly confirmed that the catalyst possessed superior thermal stability (≤200 °C), which is beneficial to maintain its catalytic activity. Magnetic property of $ZnFe_2O_4@SBA-15-ILVO_3$ catalyst was evaluated by using a VSM curve (Fig. 8**(b)**). The catalyst exhibited a superparamagnetic property with magnetic saturation 12.6 emu/g, which can be easily separated from the reaction mixture via an external magnet. In order to further expand the practicability of the protocol, the reusability of the novel catalyst was then examined for the benchmark reaction under the optimal conditions (Fig. 8**(c)**). After completion of the reaction, the catalyst could be easily separated and collected from the reaction mixture with an external magnet, washed three times with CH_2Cl_2 and subjected to the next cycle. The catalyst could be reused five times for the reaction without considerable loss of catalytic activity, indicating that the catalyst had a good catalytic recyclability. In addition, the surface appearance features of the catalyst after five cycles is similar to that of the fresh one (SEM, Fig. 2**(e)**) and the structural features of the catalyst not changed after five cycles (FT-IR, Fig. 8**(d)**), which suggested that the magnetic catalyst has excellent product performance and stability.
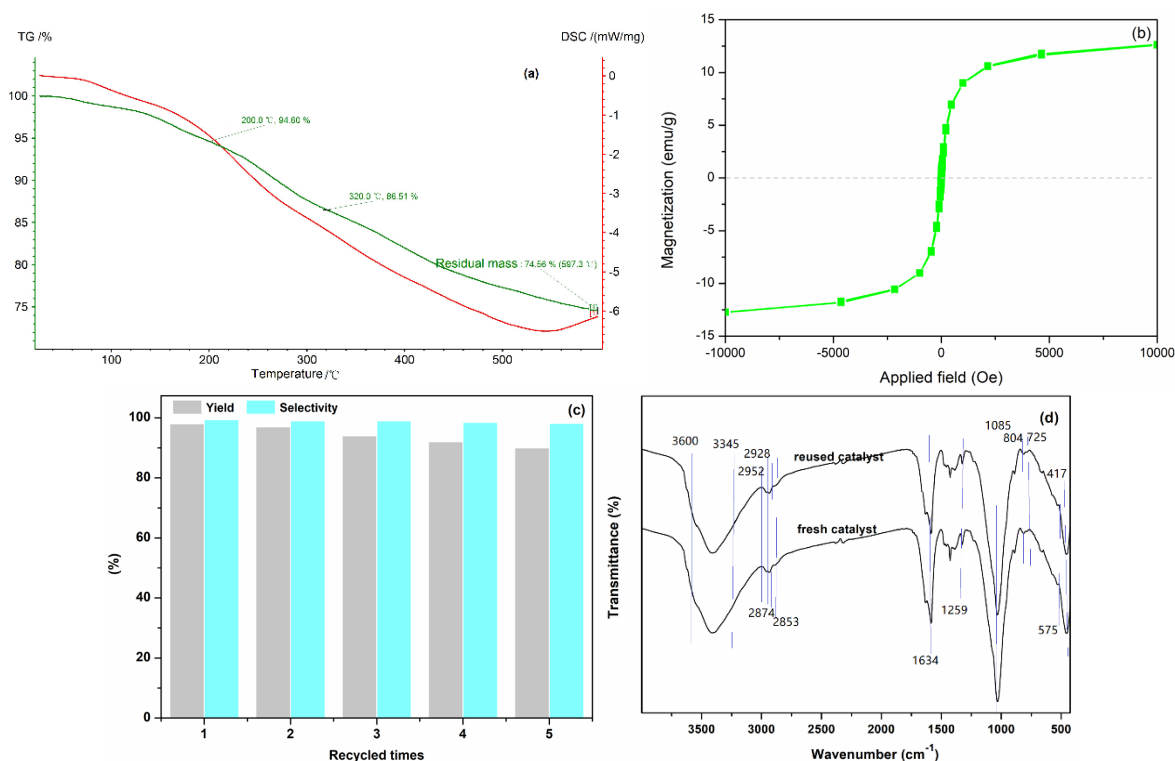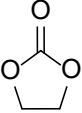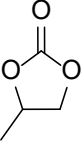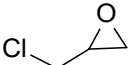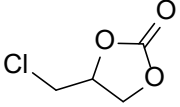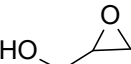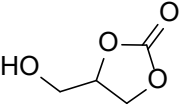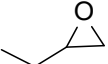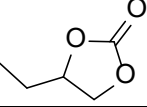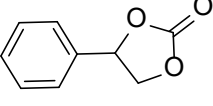

Fig. 8. (a) TG analysis, **(b)** magnetization curve, **(c)** recyclability study, and **(d)** FT-IR analysis of catalyst ZnFe2O4@SBA-15-ILVO3 after five times use.

To demonstrate the generality of this approach for the cycloaddition, a range of epoxides were then investigated (Table 2). The epoxides containing electron-donating or electron-withdrawing groups could be successfully converted into the corresponding cyclic carbonates in high to excellent yields (87~98 %) with excellent selectivities (98~99.7 %) un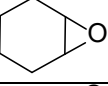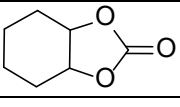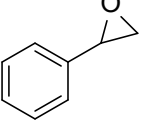der the optimal reaction conditions. Interestingly, 2-(chloromethyl)oxirane was the most reactive substrate and converted into 4-(chloromethyl)-1,3-dioxolan-2-one within 1.5 h (Table 2, entry 3). Furthermore, the carboxylation of 7-oxabicyclo[4.1.0]heptane required a long time of 4 h to obtain a high yield of 87 % (Table 2, entry 6), which may be due to the high steric hindrance during the reaction. These results indicated that the designed catalyst could be widely and efficiently used for the synthesis of cyclic carbonates through cycloaddition of CO_2 and epoxides.

**Table 2.** Catalytic synthesis of cyclic carbonates from epoxides and CO_2.[a]

Entry	Epoxide	Product	Time (h)	Yield (%)[b]	Selectivity (%)[c]
1			3	91	99.3
2			3	98	99.5
3			1.5	98	99.7
4			3	95	99.2
5			3	96	99.3
6			4	87	98
7			3	92	99.1

[a]Reaction conditions: epoxide (10 mmol), CO_2 (0.5 MPa), $ZnFe_2O_4$@SBA-15-ILVO$_3$ (0.15 g), 90 °C.
[b]Isolated yield. [c]GC analysis.

Based on the above experimental results and previous studies [15-20, 29-31], a possible reaction pathway for the catalytic synthesis of cyclic carbonates from the cycloaddition of CO_2 with epoxides was proposed (Scheme 3). The catalyst $ZnFe_2O_4$@SBA-15-ILVO$_3$ provides a synergistic microenvironment, which could be more favorable to active CO_2 and epoxides. Initially, the substrate epoxide could be activated via the coordination interaction with the metal sites of $ZnFe_2O_4$@SBA-15 support to form an intermediate **I**, together with the adsorption and activation of CO_2 by the imidazolium cation to form carbonate species. Simultaneously, the VO$_3$ anion adds to the less sterically hindered C atom of epoxide via the nucleophilic attack for the formation of intermediate **II**. Next, there is nucleophilic interaction between the oxygen anion of intermediate **II** and CO_2, thus stimulates the formation of the intermediate acyclic carbonate **III**. Subsequently, intermediate **III** could be converted into the corresponding product via intramolecular nucleophilic substitution. The regeneration of the catalyst $ZnFe_2O_4$@SBA-15-ILVO$_3$ was used for the next cycle. The presence of intramolecular synergy of ternary active sites (metal sites of $ZnFe_2O_4$@SBA-15, VO$_3$ anion, and imidazolium cation) on the CO_2 cycloaddition significantly enhanced the activities of the catalyst in this reaction system. The combination of ionic liquid and magnetic zinc ferrites modified SBA-15 provides superior advantages in the separation of cyclic carbonates products, recovery, and reusability of catalyst via an external magnet under identical conditions.
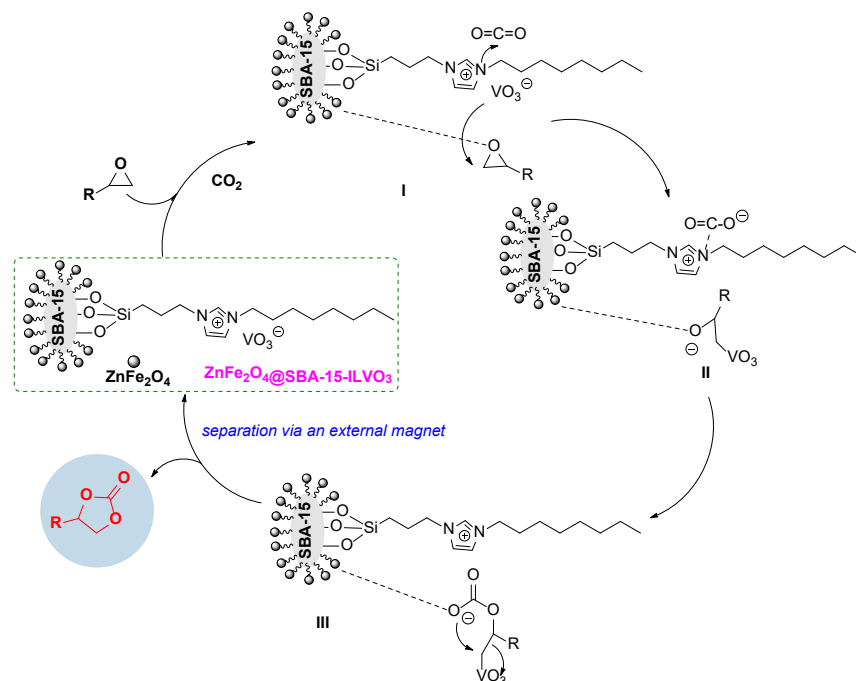
Scheme 3. Possible reaction pathway for the synthesis of cyclic carbonates.

Conclusions

In conclusion, a type of magnetic zinc ferrites modified SBA-15 supported ionic liquids were designed and synthesized and used as effective and heterogeneous catalysts for the synthesis of cyclic carbonates from epoxides and CO_2. The results showed that a range of epoxides with CO_2 employed in the presence of the catalyst $ZnFe_2O_4$@SBA-15-ILVO$_3$ leading to the corresponding products in high to excellent yields and excellent selectivities under mild conditions. Moreover, the catalyst could be easily recovered and reused for five times without a considerable decrease in catalytic activity. This procedure offers additional advantages in terms of ease work-up, feasibility, cleaner reaction profile, sustainable and stable recyclability of catalyst. This protocol provides a green and promising strategy for the synthesis of cyclic carbonates toward catalytic cycloaddition of CO_2 to epoxides.

Acknowledgements

References

1. Ji, Y.; Xu J.; Sun H.; Liu, J. *Chem. Res. Chin. Univ.* **2022**, *38*, 688-697.
2. Kassim, M. A.; Meng, T. K. *Sci. Total Environ.* **2017**, *584-585*, 1121-1129.
3. Wang, B.; Liu, J.; Yao, S.; Liu, F.; Li, Y.; He, J.; Lin, Z.; Huang, F.; Liu, C.; Wang, M. *J. Mater. Chem. A* **2021**, 9, 17143-17172.

4. Jelmy, E. J.; Thomas, N.; Mathew, D. T.; Louis, J.; Padmanabhan, N. T.; Kumaravel, V.; John, H.; Pillai, S. C. *React. Chem. Eng.* **2021**, *6*, 1701-1738.
5. Sable, D. A.; Vadagaonkar, K. S.; Kapdi, A. R.; Bhanage, B. M. *Org. Biomol. Chem.* **2021**, *19*, 5725-5757.
6. Lopes, E. J. C.; Ribeiro, A. P. C.; Martins, L. M.D.R.S. *Catalysts.* **2020**, *10*, 479.
7. Zhou, F.; Deng, Q.; Huang, N.; Zhou, W.; Deng, W. *ChemistrySelect.* **2020**, *5*, 10516-10520.
8. İkiz, M.; İspir, E.; Aytar, E.; Ulusoy, M.; Karabuğa, Ş.; Aslantaş, M.; Çelik, Ö. *New J. Chem.* **2015**, *39*, 7786-7796.
9. Muthuramalingam, S.; Velusamy, M.; Mayilmurugan, R. *Dalton Trans.* **2021**, *50*, 7984-7994.
10. Guo, F.; Zhang, X. *Dalton Trans.* **2020**, *49*, 9935-9947.
11. Beyzavi, M. H.; Stephenson, C. J.; Liu, Y.; Karagiaridi, O.; Hupp, J. T.; Farha, O. K. *Front. Energy Res.* **2015**, *2*, 1-10.
12. Nguyen, P. T. K.; Nguyen, H. T. D.; Nguyen, H. N.; Trickett, C. A.; Ton, Q. T.; Gutierrez-Puebla, E.; Monge, M. Á.; Cordova, K. E.; Gándara, F. *ACS Appl. Mater. Interf.* **2018**, *10*, 733-744.
13. Luo, R.; Yang, Y.; Chen, K.; Liu, X.; Chen, M.; Xu, W.; Liu, B.; Ji, H.; Fang, Y. *J. Mater. Chem. A* **2021**, *9*, 20941-20956.
14. Zhi, Y.; Shao, P.;   Feng, X.; Xia, H.;   Zhang, Y.; Shi, Z.; Mu, Y.; Liu, X. *J. Mater. Chem. A* **2018**, *6*, 374-382.
15. Baalbaki, H. A.; Roshandel, H.;   Hein, J. E.; Mehrkhodavandi, P. *Catal. Sci. Technol.* **2021**, *11*, 2119-2129.
16. Keshri, K. S.; Bhattacharjee, S.; Singha, A.; Bhaumik, A.; Chowdhury, B. *Mol. Catal*. **2022**, *522*, 112234.
17. Guo, C. H.; Liang, M.; Jiao, H. *Catal. Sci. Technol.* **2021**, *11*, 2529-2539.
18. Takaishi, K.; Okuyama, T.; Kadosaki, S.; Uchiyama, M.; Ema, T. *Org. Lett*. **2019**, *21*, 1397-1401.
19. Tong, H.; Qu, Y.; Li, Z.; He, J.; Zou, X.; Zhou, Y.; Duan, T.; Liu, B.; Sun, J.; Guo, K. *Chem. Eng. J.* **2022**, *444*, 135478.
20. More, G. S.; Srivastava, R. *Sustain. Energy Fuels.* **2021**, *5*, 1498-1510.
21. Valenzuela, M. L.; MacLeod-Carey, D.; Marfull, C. S.; León-Baeza, J.; Martínez, J.; Antiñolo, A.; Carrillo, F. *J. Inorg. Organomet. Polym. Mater.* 2022, 32, 1724-1735.
22. Song, Q. W.; He, L. N.; Wang, J. Q.; Yasuda, H.; Sakakura, T. *Green Chem.* **2013**, *15*, 110-115.
23. Schoepff, L.; Monnereau, L.; Durot, S.; Jenni, S.; Gourlaouen, C.; Heitz, V. *ChemCatChem.* **2020**, *12*, 5826-5833.
24. Haq, I. U.; Qasim, A.; Lal1, B.; Zaini, D. B.; Foo, K. S.; Mubashir, M.; Khoo, K. S.; Vo, D. V. N.; Leroy, E.; Show, P. L. *Environ. Chem. Lett*. **2022**, *20*, 2165-2188.
25. Fabre, E.; Murshed, S. M. S. *J. Mater. Chem. A* **2021**, *9*, 15861-15879.
26. Yan, J.; Mangolini, F. *RSC Adv.* **2021**, *11*, 36273-36288.
27. Portillo-Castillo, O. J.; Castro-Ríos, R.; Chávez-Montes, A.; González-Horta, A.; Cavazos-Rocha, N.; Granados-Guzmán, G.; de Torres, N. W.; Garza-Tapia, M. *J. Mex. Chem. Soc.* **2022**, *66*, 198-220.
28. Martínez-Palou, R. *J. Mex. Chem. Soc.* **2007**, *51*, 252-264.
29. Yan, R.; Chen, K.; Li, Z.; Qu, Y.; Gao, L.; Tong, H.; Li, Y.; Li, J.; Hu, Y.; Guo, K. *ChemSusChem.* **2021**, *14*, 738-744.
30. Zhang, J.; Li, X.; Zhu, Z.; Chang, T.; Fu, X.; Hao, Y.; Meng, X.; Panchal, B.; Qin, S. *Adv. Sustain. Syst*. **2021**, *5*, 2000133.
31. Ebrahimi, A.; Rezazadeh, M.; Khosravi, H.; Rostami, A.; Al-Harrasi, A. *ChemPlusChem.* **2020**, *85*, 1587-1595.
32. Logemann, M.; Marinkovic, J. M.; Schörner, M.; García-Suárez, E. J.; Hecht, C.; Franke, R.; Wessling, M.; Riisager, A.; Fehrmann, R.; Haumann, M. *Green Chem.* **2020**, *22*, 5691-5700.
33. Selvam, T.; Machoke, A.; Schwieger, W. *Appl. Catal. A: Gen.* **2012**, *445-446*, 92-101.
34. Cao, Y.; Zhou, H.; Li, J. *Renew. Sustain. Energy Rev.* **2016**, *58*, 871-875.

35. Xia, S. P.; Ding, G. R.; Zhang, R.; Han, L. J.; Xu, B. H.; Zhang, S. J. *Green Chem.* **2021**, *23*, 3073-3080.
36. Gandhi, S.; Sethuraman, S.; Krishnan, U. M. *Dalton Trans.* **2012**, *41*, 12530-12537.
37. Mdlovu, N. V.; Lin, K. S.; Weng, M. T.; Hsieh, C. C.; Lin, Y. S.; Espinoza, M. J. C. *J. Ind. Eng. Chem.* **2021**, *102*, 1-16.
38. Ehsanimehr, S.; Moghadam, P. N.; Dehaen, W.; Shafiei-Irannejad, V. *Colloid. Surface. A.* **2021**, *615*, 126302.
39. Laskowska, M.; Bałanda, M.; Fitta, M.; Dulski, M.; Zubko, M.; Pawlik, P.; Laskowski, Ł. *J. Magnet. Magnet. Mater.* **2019**, *478*, 20-27.
40. Karimi, B.; Tavakolian, M.; Akbari, M.; Mansouri, F. *ChemCatChem.* **2018**, *10*, 3173-3205.
41. Arora, G.; Yadav, M.; Gaur, R.; Gupta, R.; Yadav, P.; Dixit, R.; Sharma, R. K. *Nanoscale.* **2021**, *13*, 10967-11003.
42. Liu, S.; Yue, B.; Jiao, K.; Zhou, Y.; He, H. *Mater. Lett.* **2006**, *60*, 154-158.
43. Sang, C.; Jin, S.; Li, G.; Luo, Y. *J. Sol-Gel Sci. Technol.* **2021**, *98*, 559-567.
44. Zhao, Q.; Long, M.; Li, H.; Wen, Q.; Li, D. *New J. Chem.* **2022**, *46*, 1144-1157.
45. Chen, X.; Wang, P.; Xu, J.; Han, Y.; Jin, H.; Jin, D.; Peng, X.; Hong, B.; Li, J.; Yang, Y.; Ge, H.; Wang, X. *Adv. Powder Technol.* **2017**, *28*, 2087-2093.
46. Jiang, H.; Xu, X.; Zhang, R.; Zhang, Y.; Chen, J.; Yang, F. *RSC Adv.* **2020**, *10*, 5116-5128.